The Dynamics of Cavitation Bubble Collapse Impacting Fine Particles Near Spherical Wall.

[1]JAMAL-DEEN KUKURAH, [1]ANTHONY AKAYETI, [2]JOSEPH SEKYI-ANSAH, [3]JAMES KWASI QUAISIE, [3]ABDUL-HAMID MOHAMMED, [1]PHILIP YAMBA, [4]BISMARK ADDAI.

[1]Faculty of Engineering (Mechanical Engineering Department, Tamale Technical University, Tamale, GHANA
[2]Mechanical Engineering Department, Takoradi Technical University, Takoradi, GHANA
[3]Faculty of Engineering (Welding & Fabrication Department, Tamale Technical University, Tamale, GHANA
[4]Materials Engineering Department, Sunyani Technical University, Sunyani, GHANA
[*]*Corresponding author email: jkquaisie@tatu.edu.gh*

Abstract: In this article, the near ball walls cavitation bubble dynamics, collapse characteristics and particle dynamics under cavitation bubble collapse impact are studied. To effectively solve the problems of agglomeration of fine particles and grinding limit in large-scale powder preparation by mechanical method. The preparation of fine particles by cavitating jet impingement coupled with abrasive media collision was studied. From a microscopic point of view, the relationship between the breakage of quartz grains and the collapse of the micro jet and shock wave was analyzed. And target distance on cavitation intensity. According to different factors, the effect of cavitation and crushing of quartz sand ball milling on cavitation intensity was studied. The characteristics of particle size distribution were analyzed. The results indicated that in the theoretical analysis, the single cavitation bubble near the spherical wall was studied, but it will be near the actual wall. There were multiple cavitation bubble interactions, so it was necessary to further study the interaction between poly cavitation bubbles.

Keywords: cavitation bubble dynamics, impact, micro jet, intensity and spherical wall.

Received: June 19, 2022. Revised: July 21, 2023. Accepted: August 23, 2023. Published: September 19, 2023.

1. Introduction

In the process of liquid flow, the cavitation bubble suddenly increases with the ambient pressure, and its volume rapidly compresses until it collapses. When Cavitation bubbles collapse at different distances away from the wall, resulting in high-speed micro-jets and strong impact in local areas. Strike the wave. On the one hand, cavitation will lead to the damage of fluid machinery, on the other hand, there are many benefits worthy of development. The effect of near-wall cavitation bubbles on the breakdown of fine particles was worth further study. Aganin et al. [1] studied phase contact mass transfer properties' effects on the water cavitation bubble collapse. According to their findings, the influence of the mass transfer characteristics taken into account was negligible for low evaporation and condensation coefficient values and monotonically increased with their raising. In particular, the vapour mass in the bubble at the end of the collapse was overestimated by 80% if the difference between the evaporation and condensation coefficients was not taken into account, was underestimated by 10% if the temperature jump was not taken into account, and was overestimated by 20% if the non-zero ratio of the interface displacement speed due to mass exchange to the thermal motion speed of vapour molecules was ignored. Again a study on the impact phenomena caused by cavitation bubble collapse on metals and polymers was carried out by Firly et al. [2]. The air bubble was made unstable by a planar shockwave, which led to the nonspherical collapse that was frequently seen in cavitation bubbles. In metals, the impact load was largely transmitted as elastic waves of compression and shear, it was discovered by evaluating the wave propagation behavior of the bubble collapse impact load (BCIL) occurring on the surface. As a result, BCIL and acoustic impedance can be used to describe cavitation damage to metals. The Collapsing behavior of a spark-induced cavitation bubble close to the air bubble linked to the tube nozzle was studied by Tan et al [3]. Their findings demonstrate that (1) four distinct patterns may be distinguished based on the cavitation bubble's direction of collapse and how it interacts with the air bubble. (2) The cavitation bubble's dynamic characteristics, such as the collapse direction, the high-speed jet, and the shock waves, differ noticeably in different patterns. To comprehend the mechanism of air entrainment to lessen cavitation damage, it was

crucial to investigate the impact of the air bubble on the cavitation bubble. Yan et al. [4] used the pseudo-potential lattice Boltzmann method to investigate the impact of wall wettability on the process of single cavitation bubble collapse in the near-wall region. The impact pressure communicated to the hydrophilic wall without taking into account the shock-wave mechanism was of the same order as the maximum collapse pressure, whereas the impact velocity was an order lower than the maximum micro-jet velocity, according to this study. The force and the pressure around the bubble both have an impact on collapse due to wall wettability. According to preliminary investigation, the relationship between pressure differential and collapse intensity shows more patterns than we initially thought. This relationship nicely matches a logistic curve and doesn't seem to change with contact angle or initial bubble distance. Based on the Weiss theorem, Zheng et al [5]. investigated the cavitation bubble collapse and the movement characteristics of near-spherical particles. The key findings are as follows: (1) The Kelvin impulse theoretical model developed in this research was found to be able to accurately predict the movement features of the cavitation bubble near two particles of the same size based on a large number of experimental results. (2) The movement distance of the bubble centroid in the first period increases at first and then decreases when the initial bubble position is gradually moved away from the particles along the horizontal symmetry axis near two particles of the same size. (3) When the bubble centroid's initial position was at an asymmetric location near two particles, the bubble centroid's travel direction was biased toward the particle closest to the bubble but not toward its center. Base on the above previous studies, this article investigates on the influence of dimensionless distance, maximum radius of cavitation bubble and particle mass concentration was discussed. The theoretical velocity, effective dimensionless distance and maximum radius of critical cavitation bubble of fine particle impact are presented.

In order to effectively solve the problems of agglomeration and grinding limit in the preparation of fine particles by mechanical method scale, a method of preparing fine particles using a cavitating jet impact coupled with media collision was adopted in this study.

2. Methodology

2.1 Dynamic Analysis of Cavitation Bubble Collapse Impact Particles

2.1.1 Dynamic equations of cavitating bubbles

A spherical cavitating bubble of radius R with a surface energy of $4\pi\sigma R^2$, Radius expansion dR after, Its surface energy becomes $4\pi\sigma(R+dR)^2 = 4\pi\sigma R^2 + 8\pi\sigma R dR$.

So the force required for a cavitating bubble to expand is $8\pi\rho R$. According to the cavitation bubble static equilibrium equation $4\pi\sigma R^2\rho_m = 4\pi\sigma R^2\rho_B + 8\pi\sigma R$, For the bubble wall pressure there are:

$$\rho_m = \rho_B + \frac{2\sigma}{R} \quad (1)$$

Where, ρ_m - the pressure inside the bubble, Pa; ρ_B - the liquid pressure on the bubble wall, Pa;

σ- Liquid surface tension coefficient, N/m. The cavitation bubble was filled with non-condensable gases such as water vapour and air, due to the expansion of the vapour and gas in the cavitation bubble. The time of expansion and contraction is short, and the whole process can be regarded as an adiabatic process. According to the ideal gas adiabatic process, it is possible to Express as:

$$\rho_m = \rho_g + \rho_v = \rho_{g0}\left(\frac{R_0}{R}\right)^{3K} + \rho_v \quad (2)$$

From the formula, where, ρ_g - non-condensable gas partial pressure, Pa; ρ_v - Full steam pressure, Pa; ρ_{g0} - the initial pressure of the gas in the bubble, Pa; R_0 - cavitation bubble initial radius, μm; K −the adiabatic index of the gas. When the cavitation bubble expands or contracts, the volume of the surrounding liquid expands or contracts accordingly. The volume change is shown in Figure 1. The liquid volumetric kinetic energy E_K is defined as the liquid at r away from the centre of the spherical cavitating bubble and the thickness dr The kinetic energy of a spherical shell. Assuming that the liquid is incompressible, the E_K expression [6] for:

$$E_K = \frac{1}{2}\rho_f \int_R^{R_L} 4\pi r^2 \left(\frac{d_r}{d_t}\right)^2 d_r = 2\pi\rho_f R^3 \left(\frac{dR}{dt}\right)^2 \quad (3)$$

Where, ρ_f -liquid density, kg/m^3.

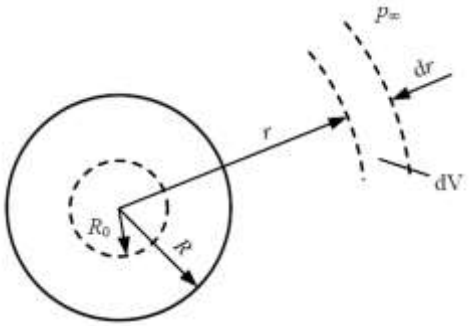

Figure 1. Cavitation bubble and liquid volume change

When a cavitating bubble expands or contracts, work is done on the surrounding liquid W_{bubble} [6] can be shown as:

$$W_{bubble} = \int_{R_O}^{R} 4\pi r^2 \rho_B dr \quad 4$$

As the volume of the cavitation bubble changes, the liquid around the cavitation bubble will also expand outward or contract inward. The work done by the volume of liquid around this cavitating bubble liquid W [6] Can be expressed as:

$$W_{bubble} = \int_{R_O}^{R} 4\pi r^2 \rho_\infty dr \quad 5$$

In formula, ρ_∞ - ambient hydrostatic pressure, Pa.

According to the energy conservation equation, the following relationship can be obtained [6]:

$$W_{bubble} = E_K + W_{liquid} \quad 6$$

By substituting (2-3) ~ (2-5) for (2-6) and taking the derivative of R, we get [6] :

$$\frac{\rho_B - \rho_\infty}{\rho_f} = \frac{2}{3}\left(\frac{dR}{dt}\right)^2 + R\left(\frac{d^2R}{dt^2}\right) \quad 7$$

When the bubble walls move, due to the viscosity of the liquid, a viscous addition term is added to equation (2-1):

$$\rho_{g_o}\left(\frac{R_O}{R}\right)^{3K} + \rho_v = \rho_B + \frac{2\sigma}{R} + \frac{4\mu}{R}\frac{dR}{dt} \quad 8$$

Liquid viscosity, Pa.s.

Finally, by substituting (2-8) for (2-7), the Rayleigh-Plesset equation is obtained [7]:

$$\frac{3}{2}\left(\frac{dR}{dt}\right)^2 + R\frac{d^2R}{dt^2} = \frac{1}{\rho_f}\left[\rho_{g_o}\left(\frac{R_O}{R}\right)^{3K} + \rho_v - \frac{2\sigma}{R} - \frac{4\mu}{R}\frac{dR}{dt} - \rho_\infty\right] \quad 9$$

2.1.2 Analysis of Cavitation Bubble Collapse Near Spherical Wall

When the pressure is reduced to the liquid-saturated vapour pressure, the liquid will vaporize, resulting in cavitation bubbles. When the pressure around the bubble recovers to the saturation steam pressure, the bubble will collapse again. Local high temperature and pressure, accompanied by high-speed micro-jets and strong shock waves are formed in bulk media [8]. In microfluidics and impingement, the shock wave appears in a different order, the micro-jets appear in the last stage of cavitation bubble contraction, while the shock wave appears in the last stage. In the rebound phase of the cavitation bubble from the minimum volume [9]. The existence of the wall has a large effect on the shape change of the cavitating bubble. With the decrease of the distance from the wall, the asymmetric collapse of the cavitation bubble produces a micro-bubble that shoots through the cavitation bubble to the wall. With the increase of the distance from the wall, the retardation of the wall was weakened and the cavitation bubble tends to symmetrical deformation. The final collapse produces a shock wave. Based on the statistical data, these two different mechanical effects will affect the Destruction efficiency.

2.1.2 The increase in the rate has a beneficial effect on:

(1) Cavitation bubble collapse micro-jets

Figure 2 shows the formation and impact of micro-jets near the spherical wall. Cavitation of maximum radius R_{max}. When the bubble moves with the water jet to the vicinity of the ball wall, the liquid movement near the bubble wall was obstructed by the ball wall, so that it was far away from the wall. The bubble wall contraction speed was faster than that near the wall, and the top of the cavitation bubble was rapidly depressed to form a vertical wall. The micro-jets, which shoot at the wall and penetrate the cavitation bubble, finally impinge on the solid wall. Due to the complexity and randomness of the cavitation bubble collapse process, it was difficult to accurately calculate the collapse micro-jets of the velocity, Plesset et al obtained an estimation formula for the micro-jets velocity V_{mjet} [10]:

$$V_{mjet} = 8.9\gamma^2\sqrt{\frac{\rho_\infty - \rho_v}{\rho_f}} \quad 10$$

Where, γ wall dimensionless distance, $\gamma = H/R_{max}$, H was the distance from the centre of the cavitation bubble to the wall, and R_{max} is the Maximum radius of the cavitation bubble. The velocity hit V_{hit} is related

to the distance between the cavitation bubble and the wall. When γ < 1, the cavitating bubble, the velocity of the micro-jet was the same as that of the wall. Erosion experiment of aluminium foil with single cavitation bubble [11]. When the brightness γ > 2.5, the micro-jets cannot damage it. Table 1 shows the numerical simulation results of cavitation bubble collapse near the wall The percentage of wall impact velocity versus micro-jets velocity at different dimensionless distances. When γ > 2.0, the wall impact velocity is Less than 10% of the micro-jet velocity; When γ = 3.0, the impact velocity on the wall is only 1.7% of the micro-jet velocity. The effect of liquid on micro-jets was obvious.

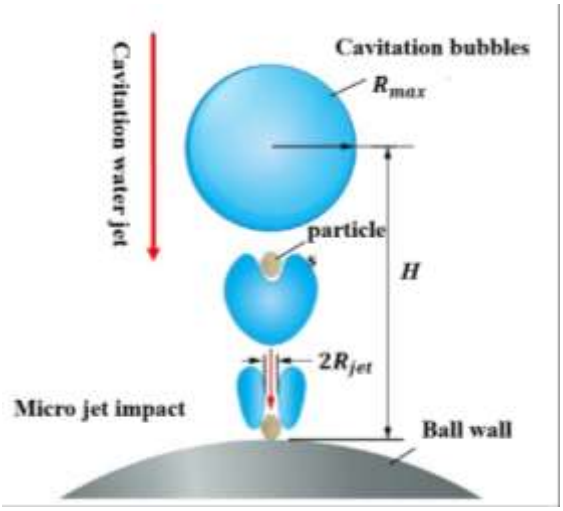

Figure 2. Formation and impact of micro-jet near-sphere wall

Table 1. The ratio of wall impact velocity to micro-jet velocity under different γ conditions [4]

Dimension distance γ	1.0	1.1	1.5	2.0	3.0
V_{hit}/V_{mjet}	100.0%	85.2%	31.8%	9.8%	1.7%

According to the data in Table 2-1, the relationship between the dimensionless distance and the velocity ratio is fitted, see Eq. (2-11):

$$\frac{V_{hit}}{V_{mjet}} = 5exp\left[\left(\frac{\gamma + 0.6659}{1.318}\right)^2\right] \quad 11$$

The vertical (10) and (11) can be combined to obtain the wall impact velocity of the micro-jets at different distances.

(2) cavitating bubble collapse shock wave

As shown in Figure 3, the cavitation bubble with a maximum radius R_{max} moves to position H from the wall, and the cavitation bubble was in the surrounding liquid. Symmetric contraction occurs under body pressure. When the cavitation bubble was compressed to the minimum radius R_{min}, the gas in the bubble bounces instantly. A strong shock wave was emitted, and the particles were accelerated by the shock wave. The numerical value of cavitation bubble collapse near the solid wall. It was found that the shock wave was dominant when γ > 1.5, and cavitation erosion can be avoided when γ > 3.0 [12]. Therefore, to make full use of the shock wave force generated by the collapse of the bubble, the effective range of the bubble and the wall was 1.5 < γ < 3.0. The Rayleigh-Plesset equation describes the radius change of a spherical cavitating bubble in the infinite domain, but when the cavitating bubble is in the collapse period the cavitation bubble will be prolonged due to the influence of the wall. Therefore, it is necessary to modify the Rayleigh-Plesset theory. The relation between the extended collapse period Tc and the dimensionless distance γ [13] for:

$$\frac{T_C}{T} = \varepsilon = 1 + 0.41\frac{1}{2\gamma} \quad 12$$

In the formula, T_C is the collapse time of the cavitation bubble near the solid wall, T is the collapse time of the spherical cavitation bubble and ε is the delay factor.

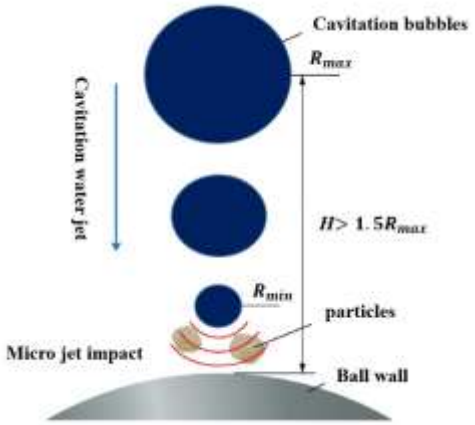

Figure 3. Shockwave action on the far side of the ball

The collapse time of a spherical cavitating bubble can be derived from the Rayleigh-Plesset equation from R = R_{max} to R = 0 integral, for the modified formula of cavitation bubble collapse time near the solid wall can be obtained:

$$T_C = 0.915_{max}\varepsilon\sqrt{\frac{\rho_f}{\rho_\infty - \rho_v}} \quad 13$$

The pressure of the shock wave at r from the centre of the cavitation bubble was calculated by equation (2-14):

$$\rho(r,t) = (\rho_\infty - \rho_v) \times \left[\frac{R}{3_R}\left(\frac{R_0^3}{R^3} - 4\right) - \frac{R^4}{3r^4}\left(\frac{R_0^3}{R^3} - 1\right)\right] \quad 14$$

3. Result and discussion

3.1 Study on Destruction of Fine Particles by Cavitation Bubble Collapse

3.1.1 Theoretical velocity analysis of particle impact fragmentation

The particles are almost not dry in the actual Destruction process, and they all contain a certain amount of pore water and surface water. In particular, in the wet grinding process, the particles are immersed in water, and the water has the function of the particle softener and grinding aid. Especially in the wet grinding process, the particles are immersed in water, and the water has particle softener and grinding aid. In practice, the compressive strength of particles was quite different from its standard compressive strength, mainly because of the small cracks, high strength, regular shape and less stress concentration of the standard mechanical specimens, so the measured standard compressive strength of the particles was much higher than the actual compressive strength. The actual compressive strength of particles can be estimated by the standard compressive strength and reduction coefficient of particles. Taking quartz sand particles in a liquid phase environment as an example, the theoretical standard compressive strength of quartz ore was 145.1~200 MPa, the compressive strength was 50 ~176.8 MPa under the condition of water immersion, and the reduction coefficient was 0.04~0.20 [60]. After considering the reduction coefficient of the compressive strength of quartz sand particles immersed in water, the actual compressive strength was 20MPa with a reasonable value. There was a "size effect" in the Destruction strength of solid particles, and the smaller the particle size was, the greater the compressive destruction strength was. The fractal model provides a theoretical analysis method for the "size effect" of particle destruction. The relationship between compressive destruction strength and particle size d is by [14].

$$\sigma_f = \sigma_f^* d^{D-3} \quad 15$$

Where f is the Intrinsic compressive strength of crushed particles, MPa, D is the Fractal dimension of particles.

According to the Destruction hypothesis proposed by Rogin, the destruction and separation of particles with a diameter of d, the destruction work Ep value is equal. Distance d from the force F_k [15]:

$$E_P = F_k \times d = \frac{1}{40}\pi\sigma_f d^2 \quad 16$$

The particles hit the wall under the impact force when the kinetic energy E_k of the impact, time was greater than or equal to particle fragmentation. When the Destruction work E_p is required, it is considered that the particles can be broken. E_k is related to the particle mass m and the particle velocity v, that is,

$$E_k = \frac{\rho_p V^2 d^3}{12} \quad 17$$

The combined vertical (2-22), (2-23) and (2-24) are available, and the particle impact wall Destruction speed meets the following conditions:

$$V \geq \sqrt{\frac{3\sigma_f d^{D-3}}{10\rho_P}} \quad 18$$

The theoretical velocity of particle breakage is related to the properties of the particle material itself, and also to the particle diameter, the smaller it was, the greater the velocity required to hit the wall.

3.1.2 Effect of dimensionless distance on cavitation bubble collapse of broken particles

When the distance between the bubble and the wall was small, the effect of the micro-jets on the wall was stronger than the shock wave. When the distance was increased to a certain extent, the effect of the micro-jets on the wall was weakened and the effect of the shock wave was weaker. The collapse process of a single cavitation bubble near the wall was analyzed more deeply, and the dimensionless distance of the wall was explored to influence the micro-jets on the wall, to determine whether the impact force of the micro-jets can cause the direct Destruction of the particles. In the cavitating jet, the micro-jets produced by the collapse of the cavitating bubble near the wall will make the particles obtain a higher velocity and increase the probability of the particles crashing into the wall. Considering that the velocity of the water jet and micro-jets was at least one order of magnitude different, the velocity of fine particles in the water jet was not considered. The diameter of the micro-jets

was not more than 10 % of the cavitating bubble diameter [16], and the diameter of micro-jets produced by millimeter-level cavitation bubble was about 100 microns, so from the perspective of momentum conservation, the diameter of particles driven by micro-jets was not more than 100 microns. Taking the quartz sand particles as an example, the density was 2650 kg/m^3, the Mohs hardness was 7, the inherent compressive failure strength was equal to 20 MPa, and the type dimension D was 2.5557 [17]. The wall impact velocity and wall dimensionless distance of quartz sand particles with different particle sizes are calculated by the combined vertical (10), eq. (11) and eq. (18). Table 2-2 lists the Destruction conditions of quartz sand particles with particle sizes in the range of 50 to 150 μm.

Table 2 Conditions of micro-jets Impact Destruction Quartz Sand Particles

Particle diameter d/μm	Impact speed $\frac{V_{hit}}{m}$ $/m/s$	Dimensions distance γ
50	92.57	1.02~1.08
75	84.59	0.98~1.24
100	79.36	0.95~1.34
125	75.52	0.92~1.39
150	72.52	0.90~1.43

From Table 2, the smaller the particle diameter, the greater the wall impact velocity required for Destruction. The more demanding it was. When the dimensionless distance was close to 1, the gravel particles of 50 μm can be broken. If broken The stone sand particles with a particle size of less than 100 μm, the speed of the particles hitting the wall should be greater than 79.36 m/s, and the wall should have no dimensional distance γ which should be between 0.95 and 1.34. A large number of cavitation bubbles because the cavitation bubble in the collapse stage was half The diameter and the distance from the wall are different, resulting in different micro-jets diameters and velocities. For fine particles, the required wall impact velocity was reduced, and the requirement for dimensionless distance was also reduced, but the micro-jets diameter was larger, so the cavitation bubble with a certain radius had a limited breaking range of fine particles, and there was an optimal breaking particle with the appropriate range.

3.1.3 Effect of the Maximum Radius of Cavitation Bubble on Collapse of Broken Particles

From the analysis of section 2.1.2, we can see that the intensity of micro-jets and shock waves produced by cavitating bubble collapse was not only affected by the dimensionless distance. It was also related to the maximum radius of the cavitation bubble. To analyze the impact fragmentation of fine particles by the maximum radius of the cavitation bubble. The effects of the collapse shock wave are first studied. Vertical (9), (13) and (14), with water as the Fluid medium having a density ρ_f of 1000 kg/m^3, 20 ºC, the saturated steam pressure ρ_v was 2340 pa, the liquid surface tension of the force coefficient σ was 0.07 N/m and the dynamic viscosity μ was 0.001 Pa.s. Initial conditions: $t = o, R_0 = R_{max,}\, \rho_{g_0} =$ 483 Pa [18], ρ_∞ = 101325 Pa, and was solved by a four-order Runge-Kutta method with variable step size. Fig. 4 shows the curves of the collapsing shock wave pressure with the distance from the center of the cavitation bubble for different maximum radius. The maximum shock wave pressure was 976 MPa, and the maximum pressure is only 0.3% different from that of Brujan [19]. The calculated pressure of 1.3 ± 0.3 GPa at the distance of 68 μm from the bubble wall using a high-speed camera technique was close to that of 1.3 ± 0.3 GPa. R_{max} has little effect on shock wave peak pressure. With the increase of the central distance r, the shock wave pressure p. The larger the R_{max} was and the smaller the k was, the slower the shock wave attenuates.

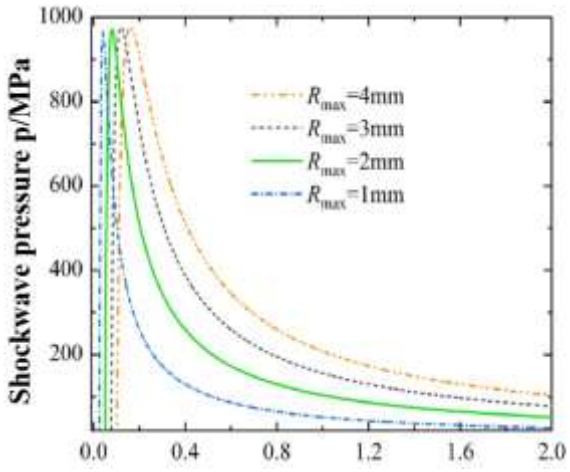

Figure 4. The pressure of the shock wave varies with the distance r of the cavitation centre

(Figure) 5 is the variation of shock wave pressure at the same position with relative time, the relative time t was relative to shock wave pressure and the time

difference between the time of the strike. In the figure, the shock wave pressure at the same position from the centre of the cavitation bubble was the peak pressure which was 52.2, 104.3, 156.3 and 208.2 MPa respectively. On the other hand, With the increase of R_{max}, the width of the shock wave becomes wider, that is when the duration becomes longer. The reason is that when the cavitation bubble collapses, the gas concentration in the cavitation bubble is different with different bubble radii, which results in a difference in shock wave pressure.

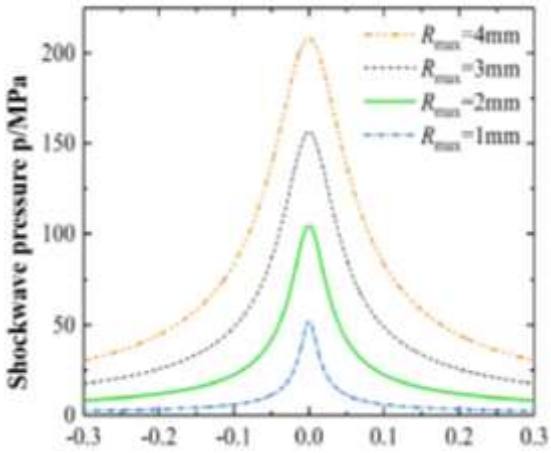

Figure 5. The pressure of shock wave changes with relative time t_r

Through the previous analysis, it can be seen that the larger the maximum radius of the cavitation bubble, the greater the intensity and duration of the collapse shock wave are. The effect of the collapse shock wave on particles was further analyzed. The quartz sand particles are also taken as an example. The curves of the maximum radius of the cavitation bubble and velocity of the particle impact wall with particle diameter are established, as shown in Fig. 6. The maximum radius of the critical cavitation bubble on the left side of Fig. 6 is defined as the radius of the cavitation bubble to reach the theoretical velocity required for particle breakage, and the longitudinal coordinate impact particle velocity on the right is the velocity of accelerating the impact on the wall after the particles are subjected to the shock wave. The maximum radius of the cavitation bubble was given when the velocity of impact particles reached the theoretical velocity required for quartz sand particle breakage. With the increase of quartz sand particle diameter, the wall impact velocity required for Destruction decreases, while the maximum radius of the critical cavitation bubble increases. The maximum radius of critical cavitation bubble for quartz sand particles with broken particle sizes of 50 μ m and 150 μ m was 1.12 mm and 1.72 mm, respectively. It could be seen that the larger the maximum radius of a cavitation bubble, the more favorable it is to breaking fine particles. The relationship between the diameter of quartz sand particles and the maximum radius of critical cavitation bubble $R'_{max} = 0.247d^{0.3864}$.

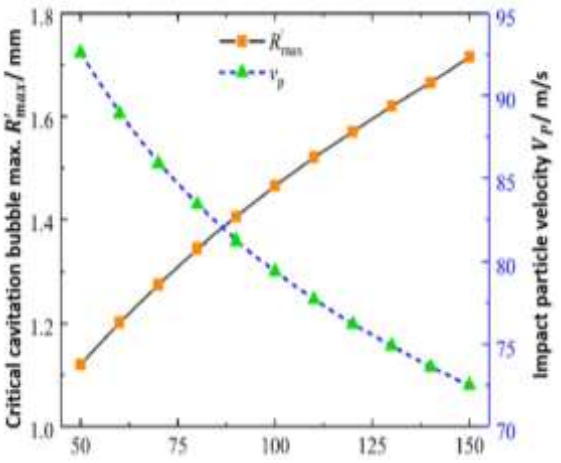

Figure 6. The maximum radius of cavitation and the velocity of particle impingement on the wall surface change with particle diameter

3.1.4 The effect of particle concentration on the collapse of cavitation bubble

With the increase of particle concentration in the liquid, more cavitation nuclei can be introduced on the other hand, thus forming more Cavitation bubbles. On the other hand, it will increase the viscosity and density of the mixed liquid, and the viscosity is the embodiment of the friction in the liquid. The influence of liquid density on the dynamics of cavitation bubbles is also very important. Therefore, it was of great significance to analyze the particle concentration for the collapse of the cavitation bubble. When the particle concentration is small, the viscosity of the two-phase fluid can be approximated to that of the fluid. When large, the viscosity of the two-phase fluid will also increase. In this case, the viscosity of the solid-liquid mixture can be calculated according to the Einstein formula [20].

$$U_S = \frac{(1 + 0.5C_m)\mu_f}{(1 - C_V)} \quad 19$$

Where, μ_s *the* viscosity of the two-phase fluid, Pa. s; C_m- particle mass concentration; C_v - particle volume

concentration; μ_f - Fluid Viscosity, Pa.so. Known particle mass concentration, the particle volume concentration can be calculated from the two-phase flow density, the two-phase fluid, The density ρ_s and the particle volume concentration C_v are respectively calculated by:

$$\rho_s = \frac{\rho_f}{1 - \left(\frac{\rho_P - \rho_f}{\rho_P}\right) C_m} \quad 20$$

$$C_V = \frac{C_m \rho_s}{\rho_P} \quad 21$$

Where, ρ_s - the density of the two-phase fluid.
Equations (19) to (21) are used to calculate the physical parameters of the two-phase fluid when the particle mass concentration was 0 ~ 15%. The results are presented in Table 3.

Table 3 Physical properties and mass concentration parameters of two-phase fluid

Particle mass concentration C_m	0%	5%	10%	15%
Particle volume C_v	0%	1.95%	4.02%	6.24%
Density of two-phase fluid $p_s/kg.m^{-3}$	1000.0	1032.1	1066.4	1103.0
Velocity of two-phase fluid $\mu_s/\ Pa.s$	0.0010	0.0011	0.0011	0.0012

As shown in Table 3, when the particle mass concentration increases, it can be found that the density of the two-phase fluid increases significantly. However, the viscosity does not change much, when C_m is in the range of 5 ≤ 10%. Visible particle mass of The concentration has little effect on the viscosity of liquid at low concentration but mainly affects the density of the two-phase liquid. From the analysis of section 3.1.2, it was known that the wall surface required for the micro-jets to break the gravel particles with a diameter of 50 ~ 150 μm was infinite. For the distance of 0.90 ~ 1.43, the influence of particle mass concentration on micro-jets velocity was established as shown in Fig. 7. With the impact curve, the increase of the particle mass concentration, the micro-jets velocity decreases due to the asymmetric collapse of the cavitation bubble. In addition, the smaller the dimensionless distance between the cavitation bubble and the wall, the particle mass concentration decreases the velocity of the micro-jets with the less degree. To analyze the effect of particle concentration on the shock wave of cavitation bubble collapse, the magnitude of the shock wave at the same location with the same radius of the cavitation bubble was compared. The maximum radius of the critical cavitation bubble for the quartz sand particles of 50 μm and 150 μm was 1.12 and 1.72 mm, respectively. Therefore, the radius of the cavitation bubble with the middle value of 1.5 mm and the distance from the centre of the cavitation bubble was 1.5 mm are selected to study the situation. The influence of particle mass concentration on shock wave pressure is shown in Fig. 8. When the particle mass concentration varies from 0% to 15%, the change of peak shock wave pressure at collapse time was minimal and almost negligible. Before and after the collapse, the shock wave pressure varies a little.

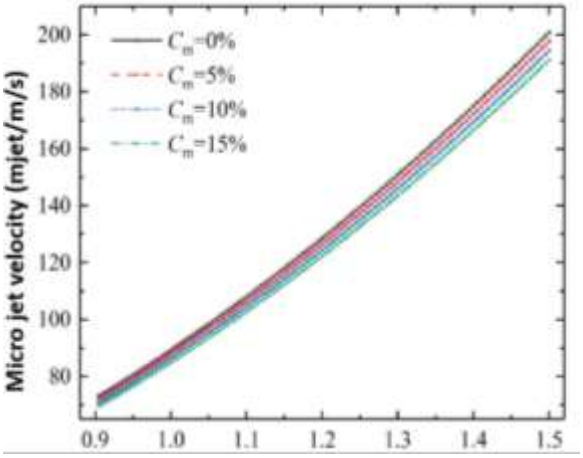

Figure 7 Effect of particle mass concentration on micro-jets velocity

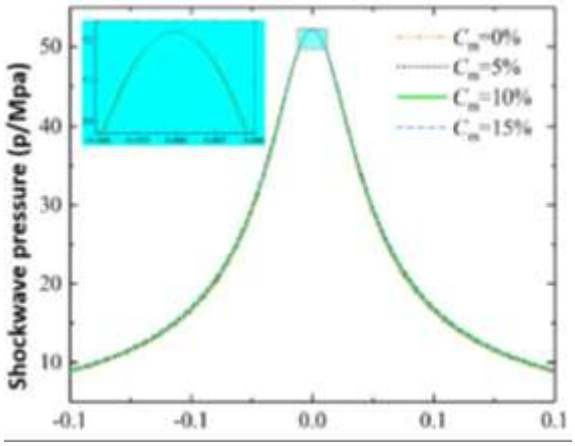

Figure 8 Effect of mass concentration of particles on shock wave pressure

4. Conclusion

The Cavitation bubble dynamics and other related theories, the velocity formula of the micro-jets impinge on the ball wall was deduced. Shock wave pressure and the kinetic equation of cavitating bubble collapse impacting fine particles in liquid were established. Based on the particle impact fragmentation theory, the wall required for effective fragmentation of 50 ~ 150 μm quartz sand particles by micro-jets was calculated. The dimensionless distance was 0.90 ~ 1.43; Critical Void Requirements for Destruction Quartz Sand Particles of 50 μm and 150 μm The maximum radius of the bubble was 1.12 mm and 1.72 mm, respectively. Foot relation R max = 0.2471 d 0.3864; By analyzing the effect of particle mass concentration on cavitation bubble collapse, it was found that with the increase of particle concentration, the collapse of the micro-jet will have a certain attenuation effect, but the shock wave pressure The impact was small. The particle mass concentration Varies in the range of 0 to 15%, resulting in the density of the two-phase granular fluid. The change of viscosity has a certain attenuation effect on the cavitating micro-jets but affects the shock wave pressure which was not big.

References

[1] A. A. Aganin and N. A. Khismatullina, "Influence of the phase interface mass transfer characteristics on the cavitation bubble collapse in water," *Ocean Engineering,* vol. 283, p. 115013, 2023/09/01/ 2023.

[2] R. Firly, K. Inaba, F. Triawan, K. Kishimoto, and H. Nakamoto, "Numerical study of impact phenomena due to cavitation bubble collapse on metals and polymers," *European Journal of Mechanics - B/Fluids,* 2023/06/12/ 2023.

[3] Z. Tan, M. Zhang, G. Huang, and B. Huang, "Collapsing behavior of a spark-induced cavitation bubble near the air bubble attached to the tube nozzle," *Ocean Engineering,* vol. 253, p. 111183, 2022/06/01/ 2022.

[4] Q. Yang, X. He, H. Peng, and J. Zhang, "Wall wettability effect on process of collapse of single cavitation bubbles in near-wall region using pseudo-potential lattice Boltzmann method," *Heliyon,* vol. 8, p. e12636, 2022/12/01/ 2022.

[5] X. Zheng, X. Wang, Z. Ding, A. Li, X. Lu, Y. Zhang, *et al.*, "Investigation on the cavitation bubble collapse and the movement characteristics near spherical particles based on Weiss theorem," *Ultrasonics Sonochemistry,* vol. 93, p. 106301, 2023/02/01/ 2023.

[6] K. Yasui and K. Yasui, *Acoustic cavitation*: Springer, 2018.

[7] A. Prosperetti, "A generalization of the Rayleigh–Plesset equation of bubble dynamics," *The Physics of Fluids,* vol. 25, pp. 409-410, 1982.

[8] S. Verma and C. Manisankar, "Shockwave/boundary-layer interaction control on a compression ramp using steady micro jets," *AIAA journal,* vol. 50, pp. 2753-2764, 2012.

[9] J. Yin, Y. Zhang, J. Zhu, L. Lv, and L. Tian, "An experimental and numerical study on the dynamical behaviors of the rebound cavitation bubble near the solid wall," *International Journal of Heat and Mass Transfer,* vol. 177, p. 121525, 2021.

[10] Y. Fu, X. Zhu, J. Wang, and T. Gong, "Numerical study of the synergistic effect of cavitation and micro-abrasive particles," *Ultrasonics Sonochemistry,* vol. 89, p. 106119, 2022.

[11] M. Dular, T. Požar, and J. Zevnik, "High speed observation of damage created by a collapse of a single cavitation bubble," *Wear,* vol. 418, pp. 13-23, 2019.

[12] A. Karimi and J. Martin, "Cavitation erosion of materials," *International Metals Reviews,* vol. 31, pp. 1-26, 1986.

[13] P. Gregorčič, R. Petkovšek, and J. Možina, "Investigation of a cavitation bubble between a rigid boundary and a free surface," *Journal of applied physics,* vol. 102, p. 094904, 2007.

[14] J. A. Bogas, M. G. Gomes, and A. Gomes, "Compressive strength evaluation of structural lightweight concrete by non-destructive ultrasonic pulse velocity method," *Ultrasonics,* vol. 53, pp. 962-972, 2013.

[15] V. M. Holers, M. K. Demoruelle, K. A. Kuhn, J. H. Buckner, W. H. Robinson, Y. Okamoto*, et al.*, "Rheumatoid arthritis and the mucosal origins hypothesis: protection turns to destruction," *Nature Reviews Rheumatology,* vol. 14, pp. 542-557, 2018.

[16] S. Song, H. Zha, G. Tian, and D. Yu, "Cavitation Phenomena on Crushing Effect of Tire under Ultra-high Pressure Water Jet," *China Mechanical Engineering,* vol. 26, p. 1205, 2015.

[17] Y. SUN, S. HUANG, Y. MAO, and L. ZHU, "Effects of ultrasonic cavitation micro jet-flow on impact fine particle breakage near rigid walls," *China Mechanical Engineering,* vol. 30, p. 2953, 2019.

[18] E. Sonde, T. Chaise, N. Boisson, and D. Nelias, "Modeling of cavitation peening: Jet, bubble growth and collapse, micro-jet and residual stresses," *Journal of Materials Processing Technology,* vol. 262, pp. 479-491, 2018.

[19] E. Brujan, T. Ikeda, and Y. Matsumoto, "On the pressure of cavitation bubbles," *Experimental Thermal and Fluid Science,* vol. 32, pp. 1188-1191, 2008.

[20] M. Duerinckx and A. Gloria, "On Einstein's effective viscosity formula," *arXiv preprint arXiv:2008.03837,* 2020.